ACS SENSORS

pubs.acs.org/acssensors

Article

Rapid Assessment of Susceptibility of Bacteria and Erythrocytes to Antimicrobial Peptides by Single-Cell Impedance Cytometry

Cassandra Troiano,[▽] Adele De Ninno,[▽] Bruno Casciaro, Francesco Riccitelli, Yoonkyung Park, Luca Businaro, Renato Massoud, Maria Luisa Mangoni, Paolo Bisegna, Lorenzo Stella,* and Federica Caselli*

Cite This: *ACS Sens.* 2023, 8, 2572−2582

Read Online

ACCESS | Metrics & More | Article Recommendations | Supporting Information

ABSTRACT: Antimicrobial peptides (AMPs) represent a promising class of compounds to fight antibiotic-resistant infections. In most cases, they kill bacteria by making their membrane permeable and therefore exhibit low propensity to induce bacterial resistance. In addition, they are often selective, killing bacteria at concentrations lower than those at which they are toxic to the host. However, clinical applications of AMPs are hindered by a limited understanding of their interactions with bacteria and human cells. Standard susceptibility testing methods are based on the analysis of the growth of a bacterial population and therefore require several hours. Moreover, different assays are required to assess the toxicity to host cells. In this work, we propose the use of microfluidic impedance cytometry to explore the action of AMPs on both bacteria and host cells in a rapid manner and with single-cell resolution. Impedance measurements are particularly well-suited to detect the effects of AMPs on bacteria, due to the fact that the mechanism of action involves perturbation of the permeability of cell membranes. We show that the electrical signatures of *Bacillus megaterium* cells and human red blood cells (RBCs) reflect the action of a representative antimicrobial peptide, DNS-PMAP23. In particular, the impedance phase at high frequency (e.g., 11 or 20 MHz) is a reliable label-free metric for monitoring DNS-PMAP23 bactericidal activity and toxicity to RBCs. The impedance-based characterization is validated by comparison with standard antibacterial activity assays and absorbance-based hemolytic activity assays. Furthermore, we demonstrate the applicability of the technique to a mixed sample of *B. megaterium* cells and RBCs, which paves the way to study AMP selectivity for bacterial versus eukaryotic cells in the presence of both cell types.

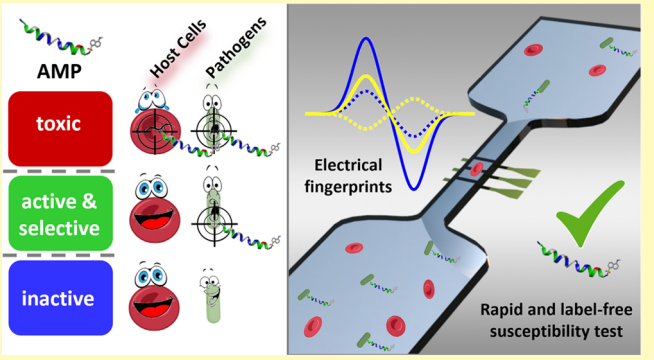

KEYWORDS: *microfluidic impedance cytometry, electrical sensing, antimicrobial peptides (AMPs), antimicrobial susceptibility testing (AST), single-cell analysis, Bacillus megaterium, erythrocyte*

Many bacterial strains are currently resistant to several, or even all, available antibiotics. Bacterial resistance to antimicrobial drugs (AMR, for antimicrobial resistance) is a major threat to human health and has been termed an "overlooked pandemic".[1] More than one million deaths are currently directly attributable to AMR, a value that ranks behind only COVID-19 and tuberculosis in terms of global deaths from an infection.[2] In addition, the declining efficacy of existing antibiotics is endangering many essential procedures in modern medicine (including surgery, chemotherapy, organ transplantation, etc.) that require effective antimicrobial drugs.[3] The problem of AMR is exacerbated by the lack of development of new antibiotics: the last entirely original class of antibiotics was discovered in the late 1980s.[4]

Antimicrobial peptides (AMPs), sometimes also called host defense peptides, are a particularly promising class of molecules to fight AMR.[5] They are natural molecules produced by all organisms, including humans, as a first line of defense against invading pathogens.[6] They have a broad spectrum of activity, low toxicity against host cells, and usually kill bacteria in a few minutes by making their membranes permeable.[7,8] Due to this mechanism of action, the development of resistance against AMPs is particularly difficult.[9]

Antimicrobial susceptibility testing (AST), which assesses the susceptibility of pathogens to antimicrobial drugs, is a key factor in the treatment of bacterial infections and in the fight against antibiotic resistance. AST can allow the prescription of appropriate drugs and, therefore, a reduction in the use of

Received: February 10, 2023
Accepted: June 26, 2023
Published: July 8, 2023

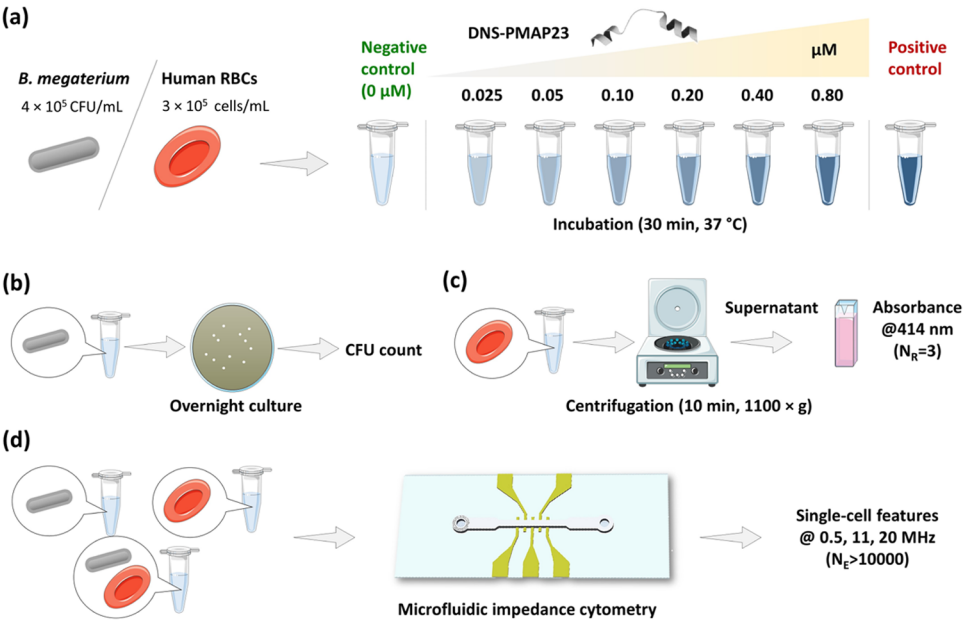

Figure 1. Overall experimental protocol. (a) Sample preparation: *B. megaterium* cells and human RBCs were incubated at 37 °C for 30 min with the DNS-PMAP23 peptide at six different concentrations in the range of 0.025−0.80 μM. As negative control, samples without peptide were prepared. As positive control, samples with peptide concentration over 1 μM (for the bacteria) or samples treated with osmotic shock (for the RBCs) were prepared. (b) Standard bactericidal assay: colony-forming unit (CFU) count after overnight culture. (c) Standard RBC hemolysis assay: absorbance measurements at 414 nm of supernatant after centrifugation (N_R, number of replicates). (d) Microfluidic impedance cytometry: bacterial suspensions, RBC suspensions, or mixed samples were measured with an impedance cytometer at 0.5, 11, and 20 MHz stimulation frequency. Thousands of single cells were acquired for each experimental condition (N_E, number of events).

broad-spectrum antibiotics. However, current methods require overnight incubation, while a rapid response is critical in the effective treatment of infections. Therefore, there is an urgent need for faster AST methods.[10,11] Also in the specific case of AMPs, researchers agree on the necessity of improving AST methods.[12] For instance, selectivity for bacterial versus eukaryotic cells is an essential characteristic of AMPs, in view of therapeutic applications. This property arises from the different compositions of the membranes of the two cell types.[13] However, some of us recently showed that the standard assays used to assess selectivity (separate experiments on human and bacterial cells, at fixed cell densities) are not representative of the real conditions encountered in vivo.[14,15] The development of approaches where antibiotic activity and toxicity are assessed in the presence of both cell types is essential.[16] Another limit of current AST methods is that measurements on bacterial populations are not suited to investigate the presence of a small number of persister or viable but nonculturable cells, which are crucial in preventing the eradication of the infection by antimicrobials. Cell-to-cell differences in drug response within a clonal bacterial population have also been reported in the case of AMPs.[15,17−20] Single-cell techniques are required to address cell heterogeneity.[21]

Microfluidic impedance cytometry is particularly suited to address the needs of short analysis times and of information at the single-cell level. Its merits with respect to current state-of-the-art AST methods are comprehensively discussed by Spencer et al.[22] The technique measures the electrical phenotype of individual biological cells and has been applied to mammalian cells, human pathogens, yeast cells, and plant cells.[23−30] The sensitivity of the technique to alterations of cell size, membrane, and interior composition makes it particularly suitable for cell viability applications.[31−34] David et al.[35] performed impedance-based viability analysis of *Bacillus megaterium* with cells at different growth stages and heat-inactivated cells. Bertelsen et al.[36] showed that the impedance response of *Escherichia coli* depends on its viability state, but the specific response depends on the inactivation method (ethanol, heat, or autoclavation). Impedance-based systems for susceptibility assessment of bacteria at the single-cell level were recently reported[22,37,38] (cf. Table S1 for details). Tang et al.[37,38] showed an increase in the volume of *E. coli* cells susceptible to treatment with Mecillinam. Spencer et al.[22] used microfluidic impedance cytometry to test bacterial susceptibility to traditional antibiotics and showed that the measured electrical characteristics reflect the phenotypic response of the bacteria to the mode of action of a particular antibiotic. They also tested the activity of the bacterial, cyclic lipopeptide colistin, which is membrane-active. However, to the best of our knowledge, no impedance data are available on the activity of gene-encoded, linear AMPs, belonging to the innate immune system of multicellular organisms, nor on their toxicity toward host cells.

In this paper, we present the use of microfluidic impedance cytometry to investigate the activity of AMPs on both bacteria and human cells. The peculiar mechanism of action of AMPs makes them particularly amenable to studies based on this technique. Cellular effects of AMPs are predicted to produce measurable changes in impedance values, since they include perturbation of cell membrane permeability, dissipation of transmembrane gradients, loss of intracellular material, and changes in cell volume/shape.[7,17,39,40] In addition, in the case of bacteria, after membrane perturbation, AMPs accumulate inside dead cells,[17,19,41,42] binding to intracellular components[43] and causing rigidification of the cytosol.[44,45]

We selected porcine cathelicidin PMAP-23 as a representative example of AMPs. PMAP-23 is a 23-residue, linear,

https://doi.org/10.1021/acssensors.3c00256
ACS Sens. 2023, 8, 2572−2582

amphipathic peptide, produced by pig myeloid cells,[46] endowed with antibacterial,[46] antifungal,[47] and antinematodal activities.[48] PMAP-23 kills bacteria by perturbing the permeability of their membranes. It forms pores according to the so-called "carpet" mechanism,[8,49,50] where peptides accumulate on the membrane surface, perturbing its surface tension and causing the formation of defects once a threshold of bound peptide molecules is reached. After the disruption of bacterial membranes, PMAP-23 binds with high affinity to intracellular components.[43] In recent years, we used a fluorescently labeled analogue of PMAP-23 (indicated as DNS-PMAP23, due to the presence of a dansyl label at the N-terminus) to quantitatively characterize its interaction with bacterial and human cells.[8,14,43] For this reason, DNS-PMAP23 was selected for the present study, too. We have previously shown that bacterial killing and hemolysis by DNS-PMAP23 are fast, being completed in less than 15 min.[14] In the present study, the bactericidal activity of DNS-PMAP23 was tested on *B. megaterium* cells, which are commonly used as Gram-positive bacterial model organisms.[35] The hemolytic activity of the peptide on purified human red blood cells (RBCs) was also investigated since this is the most commonly used measure of AMP cytotoxicity and selectivity[13] and allows comparison with our previous studies.[14]

The overall experimental protocol is illustrated in Figure 1 (see Materials and Methods Section for details). Bacterial and RBC samples at different peptide concentrations were prepared (Figure 1a) and characterized with reference approaches—a CFU counting assay for the bacterial samples (Figure 1b) and an absorbance-based hemolysis assay for the RBC samples (Figure 1c)—in parallel to microfluidic impedance cytometry analysis (Figure 1d).

The results show that impedance-based metrics can be used as indicators of AMP-induced cell alterations. Specifically, the impedance phase at high frequency (e.g., 11 or 20 MHz) turns out to be a reliable label-free metric for monitoring AMP bactericidal activity and toxicity to host cells. Furthermore, a proof-of-concept experiment involving a mixture of *B. megaterium* and RBCs, either incubated with the peptide or untreated, was performed. The simultaneous analysis of bacteria and host cells is critical to study peptide selectivity under realistic conditions. To the best of our knowledge, this is the first time that impedance cytometry is used to characterize a mixture of bacteria and human cells. Overall, these results support the use of microfluidic impedance cytometry for the selection of the most effective AMPs exhibiting maximum activity and minimum toxicity in the presence of mixed cell populations.

MATERIALS AND METHODS

Materials. DNS-PMAP23 (dansyl-RIIDLLWRVRRPQKPKFVTVWVR-NH_2), labeled with 5-(dimethylamino)naphthalene-1-sulfonyl (dansyl) at the N-terminus and amidated at the C-terminus, was purchased from AnyGen Co. (Gwangju, South Korea).

The Gram-positive bacterium *B. megaterium* Bm11 was kindly provided by Prof. Hans G. Boman (MTC, Karolinska Institute, Sweden). Red blood cells were collected from blood samples obtained from healthy volunteers.

Sample Preparation. *B. megaterium* Bm11 was grown in LB (Luria-Bertani broth) medium at 37 °C in an orbital shaker until a mid-log phase was reached, as indicated by absorbance of 0.8 at 590 nm. Bacterial cells were centrifuged (1400*g* for 10 min, Eppendorf 5702 centrifuge, Hamburg, Germany) and washed eight times in buffer A (5 mM HEPES, pH = 7.3, 110 mM KCl, 15 mM glucose) to remove traces of LB medium. The cells were then resuspended in buffer A.[43] Control experiments, performed in the absence of the peptide, with ~3 × 10^7 colony-forming units (CFU) per mL, demonstrated that in this minimal medium, where bacteria are viable but do not multiply, the density of CFU remained constant, within experimental errors, for at least 2 h, both at 25 and 37 °C, thus maintaining a constant density of live cells in the timeframe of the experiments. Bacterial cells were diluted in buffer A to a final cell density of 4 × 10^5 CFU/mL and were incubated with DNS-PMAP23 at different concentrations (from 0.025 to 0.80 μM) at 37 °C for 30 min. Total bacterial killing (positive control) was obtained by using a high peptide concentration (>1 μM). Negative control was obtained by suspending bacterial cells in buffer A, without any peptide. Bacterial samples were analyzed in parallel via a standard antibacterial activity assay and via microfluidic impedance cytometry.

Blood from healthy donors was washed six times with 5 mM HEPES, pH 7.3, 150 mM NaCl (buffer E), and resuspended in the same buffer. After this step, RBC density was measured with an automated hematology analyzer Sysmex XE-2100 (TOA Medical Electronics, Kobe, Japan). Aliquots of the RBC suspension, diluted in buffer A at a final concentration of 3 × 10^5 cells/mL, were incubated with six different concentrations of DNS-PMAP23 (from 0.025 to 0.80 μM), at 37 °C for 30 min. Negative control was obtained by suspending RBCs in buffer A, without any peptide. Total hemolysis (positive control) was obtained by suspending RBCs in distilled water overnight (osmotic shock). The RBC samples were analyzed in parallel via a standard hemolytic activity assay and via microfluidic impedance cytometry.

A mixed sample containing both bacterial cells and RBCs suspended in buffer A at concentrations of 4 × 10^5 CFU/mL and 3 × 10^5 cells/mL, respectively, was also prepared. An aliquot of this suspension was treated with peptide incubation (0.35 μM) at 37 °C for 30 min. The untreated and treated mixed samples were analyzed via microfluidic impedance cytometry.

Antibacterial Activity Assay. After peptide incubation, aliquots of 5 μL of bacterial cell suspension were withdrawn, diluted in buffer A to optimize the cell density for colony counting, and spread onto LB-agar plates for counting after overnight incubation at 37 °C. Survival (S) of bacterial cells was expressed as a fraction with respect to the untreated sample: $S = \mathrm{CFU}/\mathrm{CFU}_{\mathrm{NC}}$ (where the subscript NC denotes the negative control sample). The percentage of bacterial killing was calculated as follows

$$\text{killing}\ (\%) = [1 - S] \times 100 \tag{1}$$

The Hill model

$$y = \frac{100}{1 + \left(\frac{K}{x}\right)^n} \tag{2}$$

was fit to the datapoints. Here x denotes the peptide concentration. The parameter K is the peptide concentration corresponding to half bacterial killing, whereas the parameter n is the Hill coefficient, which is an indicator of the cooperativity of peptide binding to cells.

Hemolytic Activity Assay. The hemolytic activity of DNS-PMAP23 was measured on human RBCs, following the previously published protocol.[14] Briefly, after peptide incubation, the RBC samples were centrifuged in a Spectrafuge 24D (Labnet International Inc, Edison, NJ) for 10 min at 1100*g*, and the absorbance (Abs) of the supernatant was measured on a Cary-UV 100 Scan spectrophotometer (Varian, Middelburg, Netherlands) at 414 nm (i.e., the wavelength of maximum absorbance of the Soret band) using 1 cm pathlength cuvettes.

Hemoglobin release was calculated as follows

$$\text{hemoglobin release}\ (\%) = \left[\frac{\mathrm{Abs} - \mathrm{Abs}_{\mathrm{NC}}}{\mathrm{Abs}_{\mathrm{PC}} - \mathrm{Abs}_{\mathrm{NC}}}\right] \times 100 \tag{3}$$

https://doi.org/10.1021/acssensors.3c00256
ACS Sens. 2023, 8, 2572−2582

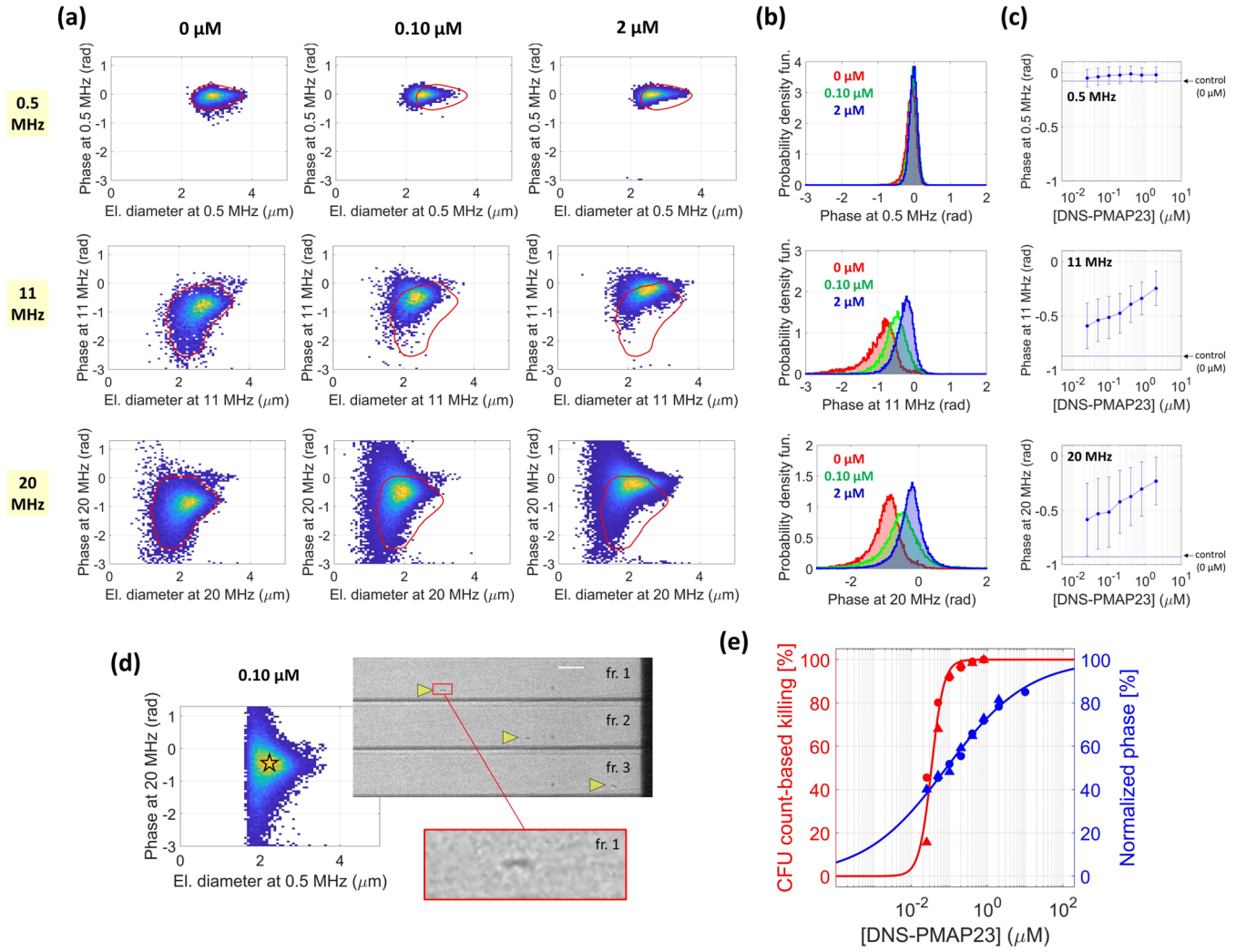

Figure 2. Results of the *B. megaterium* analysis. (a) Impedance-based characterization of *B. megaterium* cells at 0.5 MHz (first row), 11 MHz (second row), and 20 MHz (third row) stimulation frequencies. The density plot of the phase against the electrical diameter is shown for the negative control sample (0 μM, first column), the sample at 0.10 μM (second column), and the sample at 2 μM (third column). For each stimulation frequency (i.e., in each row), the red contour line in the first column denotes the region enclosing 95% of the datapoints of the negative control sample (0 μM). This contour line is plotted as a reference also in the density plot of the samples at 0.10 μM (second column) and 2 μM (third column). (b) Empirical probability density function of the phase at 0.5 MHz (first row), 11 MHz (second row), and 20 MHz (third row) for the samples at 0 μM (in red), 0.10 μM (in green), and 2 μM (in blue). (c) Median values of the phase at 0.5 MHz (first row), 11 MHz (second row), and 20 MHz (third row) as a function of the peptide concentration. Interquartile ranges are also shown. In each panel, the horizontal line indicates the median value of the phase of the negative control sample (0 μM). (d) Density plot of the phase at 20 MHz against the electrical diameter at 0.5 MHz (sample at 0.10 μM), along with exemplary snapshots of a flowing *B. megaterium* cell (three consecutive frames, fr.; scale bar is 20 μm). (e) Comparison of the killing curve based on microfluidic impedance cytometry (at 20 MHz), in blue, with the killing curve based on CFU counts, in red. Markers denote experimental datapoints (circles and triangles refer to different experiment repetitions), and continuous lines denote fits of the results.

where the subscript PC denotes the positive control sample. Datapoints were obtained as the mean of three independent measurements. The Hill model (eq 2) was fit to the datapoints.

Microfluidic Impedance Cytometry. The microfluidic impedance chip (Figure S1) consisted of a PDMS fluidic layer sealed to a microscope glass slide (75 mm × 25 mm) patterned with microelectrodes (Ti/Au, 20/200 nm). Standard techniques were used for device microfabrication, as previously described.[51] In the electrical sensing zone, the channel width and channel height were 40 and 20 μm, respectively. Electrodes were 30 μm wide in the flow direction, with a 10 μm spacing. Electrodes of similar dimensions were previously used to characterize RBCs[51,52] or bacteria.[22,37,38] Further design optimization could be possible,[53,54] but this would not be straightforward in the case of size heterogeneous samples.

A three-electrode differential measurement scheme was used (Figure S1a): alternating current (AC) voltage was applied to the central electrode; the currents flowing through the lateral electrodes were conditioned by a transimpedance amplifier (HF2TA, Zurich Instruments) and sent as input to an impedance spectroscope (HF2IS, Zurich Instruments, 115 kHz sampling rate); the spectroscope performed lock-in demodulation and the demodulated differential signals were saved into a PC for subsequent signal processing. Measurements at 0.5, 11, and 20 MHz stimulation frequency were performed. The low-frequency value of 0.5 MHz is commonly used to probe the cell size, while the high-frequency values (11 and 20 MHz) were chosen as a compromise between their ability to probe the cell membrane/cytoplasm and good signal-to-noise ratio.[23]

https://doi.org/10.1021/acssensors.3c00256
ACS Sens. 2023, 8, 2572−2582

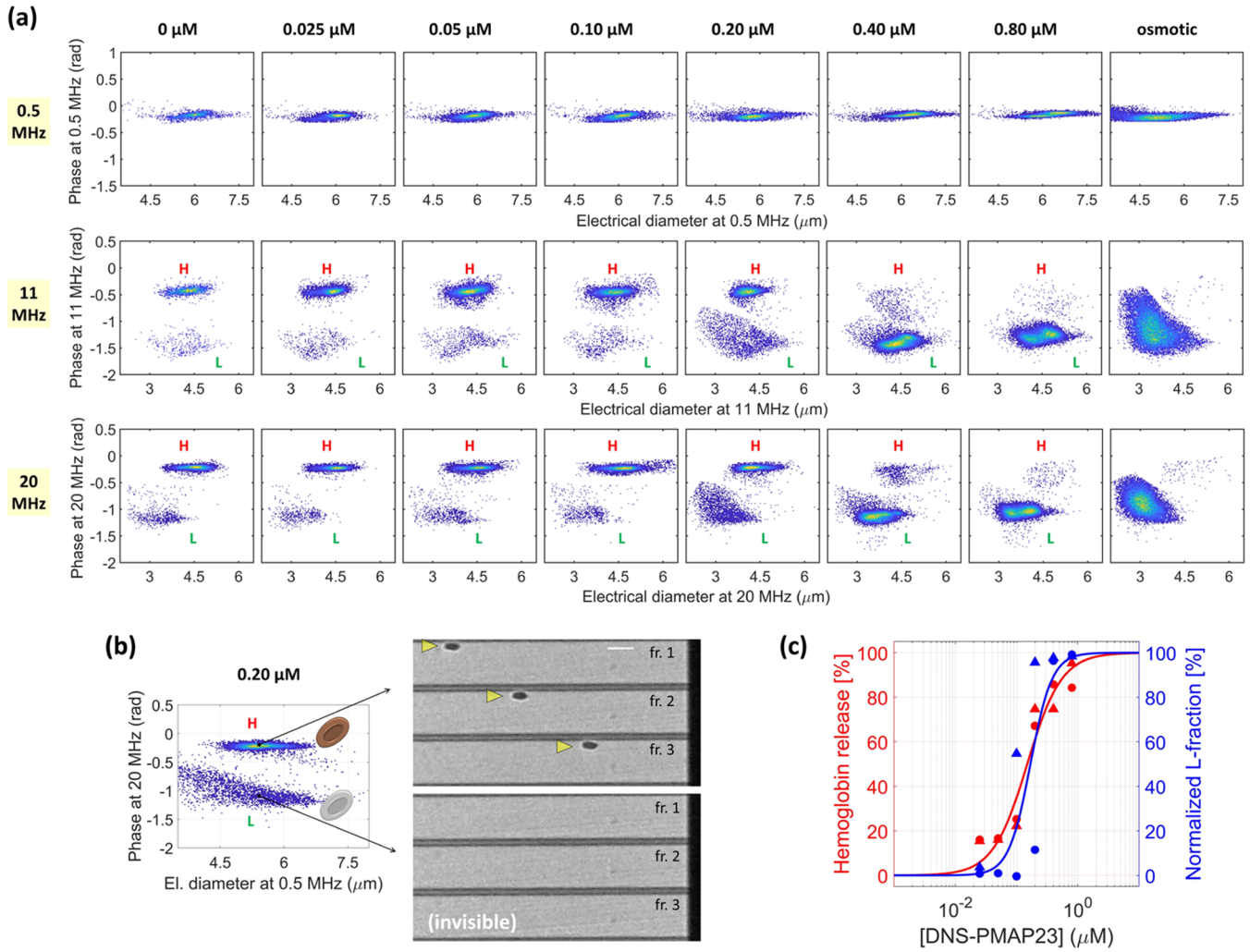

Figure 3. Results of the RBC analysis. (a) Impedance-based characterization of RBCs at 0.5 MHz (first row), 11 MHz (second row), and 20 MHz (third row). For each peptide concentration (column-by-column), the density plot of the phase against the electrical diameter is shown (last column refers to the osmotic sample). Two RBC populations are found at 11 and 20 MHz, denoted by H (high phase) and L (low phase). (b) Density plot of the phase at 20 MHz against the electrical diameter at 0.5 MHz (sample at 0.20 μM). RBCs of subpopulation *H* are clearly detectable in the high-speed video (three consecutive frames, fr.; scale bar is 20 μm). RBCs of subpopulation *L*, despite having comparable electrical size, resulted invisible with the present optical setup. (c) Comparison of the RBC toxicity assay based on microfluidic impedance cytometry (at 20 MHz), in blue, with the standard toxicity assay based on hemoglobin release, in red. Markers denote experimental datapoints (circles and triangles refer to RBCs from two different donors), and continuous lines denote fits of the results.

Before the measurements, the samples were spiked with polystyrene beads (4.5 μm diameter, Polyscience) at a concentration of about 2×10^5 beads per mL as an internal reference. A syringe pump (Harvard Apparatus) was used to inject the samples into the microfluidic chip (10 μL/min flow rate).

The nominal values of sample concentrations and flow rate yield a nominal acquisition throughput in the range of 80−150 particles per second, which was confirmed by the analysis of the recorded data streams (i.e., dividing the number of detected particles by the acquisition time). Accordingly, for each experimental condition, thousands of single-cell events were measured in a few minutes. Higher acquisition throughput could be achieved by increasing the sample concentration or the flow rate; however, this would require strategies to handle coinciding events[51] or higher sampling rate, respectively.

A bipolar Gaussian template was fit to each event detected in the data stream (cf. Figure S2 for details). Electrical diameter (i.e., cube root of peak amplitude) and phase were computed at each stimulation frequency. Bead signals were used to calibrate those features (i.e., the average electrical diameter of the bead population was set to 4.5 μm, and the average bead phase was set to zero) to enable quantitative comparison between measurements.[55] The present chip layout is subject to position-induced blurring due to the nonuniformity of the electric field in the vertical direction.[56] However, the electrical diameter enabled the distinction between bacteria and RBCs in the mixed sample experiment, and the phase feature turned out to be only slightly affected by the particle position (the standard deviation of the bead phase was 0.03 rad).

The whole processing workflow was implemented in a custom MATLAB script running on a processor Intel(R) Xeon(R) CPU E5-2640 v3@2.60GHz with 64 GB RAM. The average processing throughput was 120 events per second. As a further development, faster approaches based on machine learning[37,57,58] could be implemented.

The normalized phase of the bacterial population was calculated as follows

$$\text{normalized phase (\%)} = \left[\frac{\text{Ph} - \text{Ph}_{\text{NC}}}{\text{Ph}_{\text{PC}} - \text{Ph}_{\text{NC}}}\right] \times 100 \quad (4)$$

where Ph denotes the median phase. As detailed in the Results Section, the impedance-based analysis of the RBCs revealed the

https://doi.org/10.1021/acssensors.3c00256
ACS Sens. 2023, 8, 2572−2582

presence of two subpopulations, labeled as subpopulation H and subpopulation L. Denoting by f_L, the relative fraction of RBCs belonging to subpopulation L, the normalized fraction of L-subpopulation was calculated as follows

$$\text{normalized } L\text{-fraction } (\%) = \left[\frac{f_L - f_{L,\text{NC}}}{f_{L,\text{PC}} - f_{L,\text{NC}}}\right] \times 100 \quad (5)$$

In analogy with the standard antibacterial and hemolytic activity assays, the Hill model (eq 2) was used to fit the electrical signatures (namely, the normalized phase (eq 4) and normalized L-fraction (eq 5)).

Image Acquisition. With the purpose of optically controlling the passage of cells in the microchannel, the sample flow through the electrical sensing zone was acquired with a high-speed video microscopy system (Photron Mini UX100 camera operating at 4000 fps, 3.9 μs shutter time; Zeiss Axio Observer microscope with 20× objective), simultaneously to impedance acquisition, as described in previous works.[59,60]

RESULTS

Impedance-Based Characterization of *B. megaterium* Cells under Peptide Exposure. The results of the impedance-based characterization of *B. megaterium* cells exposed to the DNS-PMAP23 peptide are collected in Figure 2. Figure 2a shows the density plots of the phase against the electrical diameter, at each stimulation frequency (0.5, 11, and 20 MHz), for the negative control (i.e., 0 μM, no peptide), a sample at 0.10 μM, and a sample at high peptide concentration (i.e., 2 μM). In the negative control sample (first column), at low frequency (0.5 MHz), the electric diameter falls in the range of 2.5−3.5 μm and the phase is close to zero (i.e., the phase of reference beads). Both the electrical diameter and the phase diminish by increasing the frequency from 0.5 MHz to 11 or 20 MHz. The effect of peptide incubation mainly affects the phase at high frequency. Specifically, at 11 or 20 MHz, the addition of the peptide induces a shift of the phase from negative values toward zero. On the other hand, at low frequency (0.5 MHz), the phase remains rather stable with peptide exposure. These trends are further visualized in Figure 2b, reporting the corresponding empirical probability density function of the phase at each frequency. The behavior of the phase across the whole set of tested peptide concentrations (i.e., 0, 0.025, 0.05, 0.10, 0.20, 0.40, 0.80, and 2 μM) is shown in Figure 2c, where the median phase values and the interquartile ranges are reported. The sensitivity to peptide exposure of the phase at high frequency (11 or 20 MHz) is confirmed.

By using the impedance signals as pointers to image frames,[59] bacterial cells could be automatically identified in the acquired high-speed videos. Exemplary snapshots of an individual bacterial cell flowing through the microfluidic cytometer are shown in Figure 2d. The optical setup used to acquire images of flowing cells has a limited resolution and does not allow an accurate evaluation of bacterial morphology, which is typically performed via scanning electron microscope (SEM) images of static cells. Exemplary SEM images of untreated and treated *B. megaterium* cells are reported in Figure S3. They show that the bacterial size and overall shape were not significantly affected by treatment with the peptide, in agreement with the lack of significant changes in the electric diameter, and with the mechanism of action of DNS-PMAP23, which is based on pore formation in the cell membranes.

The standard assay for determining peptide bactericidal activity is based on CFU count after overnight culture. The corresponding bacterial killing (eq 1) at different peptide concentrations is reported in red in Figure 2e. The relevant fit (eq 2) is also shown (parameter values, mean ± std: K = 0.034 ± 0.003 μM, n = 2.7 ± 0.6). The CFU-count-based method shows that *B. megaterium* is susceptible to the DNS-PMAP23 peptide, since the number of bacterial cells able to form colonies diminishes for increasing peptide concentration. The phase at a high frequency is sensitive to peptide exposure, and hence it is a potential biomarker of peptide bactericidal activity that does not require bacterial cultures. The normalized phase (eq 4) at different peptide concentrations is reported in blue in Figure 2e, along with the corresponding fit (parameter values: K = 0.08 ± 0.03 μM, n = 0.40 ± 0.06). The bacterial killing caused by the treatment with DNS-PMAP23 at increasing concentration is reflected in an increase of the normalized phase.

Impedance-Based Characterization of RBCs under Peptide Exposure. The results of the impedance-based characterization of RBCs exposed to the DNS-PMAP23 peptide are collected in Figure 3. As a representative example, Figure 3a shows the density plots of the phase against the electrical diameter, at each stimulation frequency (0.5, 11, and 20 MHz), for the negative control (i.e., 0 μM, no peptide), the samples incubated at different peptide concentrations (0.025, 0.05, 0.10, 0.20, 0.40, 0.80 μM), and the positive control (osmotic shock). The peptide concentrations were selected to properly sample the range where DNS-PMAP23 was previously shown to be hemolytic.[14] At low frequency (0.5 MHz), the electrical features do not exhibit a noticeable trend with respect to peptide exposure. For all samples, the electrical diameter at 0.5 MHz falls in the range of 4.5−7.5 μm, and the phase is slightly lower than that of the reference beads (i.e., around −0.2 rad). At a high frequency (11 or 20 MHz), lower electrical diameters are measured (2.5−6 μm range) and a distinctive behavior is found, characterized by the presence of two RBC subpopulations having different phases.

The subpopulation with a higher phase is denoted by H and the one with lower phase is indicated by L. Subpopulation L also exhibits a noticeable reduction of the electrical diameter at 20 MHz compared to that at 11 MHz. The relative fraction of the two subpopulations varies across the samples. In the negative control sample (0 μM) and at low peptide concentration (up to 0.10 μM in this representative example), subpopulation H is markedly dominant. At 0.20 μM, both subpopulations are well represented, whereas at 0.40 and 0.80 μM, subpopulation L is markedly dominant. The positive control exhibits one population, which has electrical signatures close to those of subpopulation L (even though they are not completely overlapping).

Subpopulations H and L, despite having comparable electrical size (i.e., electrical diameter at 0.5 MHz), turned out to be different at optical inspection (Figure 3b). Whereas cells belonging to subpopulation H were clearly identifiable in the recorded high-speed videos, cells belonging to subpopulation L turned out to be invisible. Cells of the positive control were not optically detectable, with the present optical setup, either.

The standard assay for determining peptide toxicity to RBCs is based on the quantification of hemoglobin release, as measured by absorbance levels in a sample where RBCs have been removed by centrifugation. Figure 3c shows, in red, the

https://doi.org/10.1021/acssensors.3c00256
ACS Sens. 2023, 8, 2572−2582

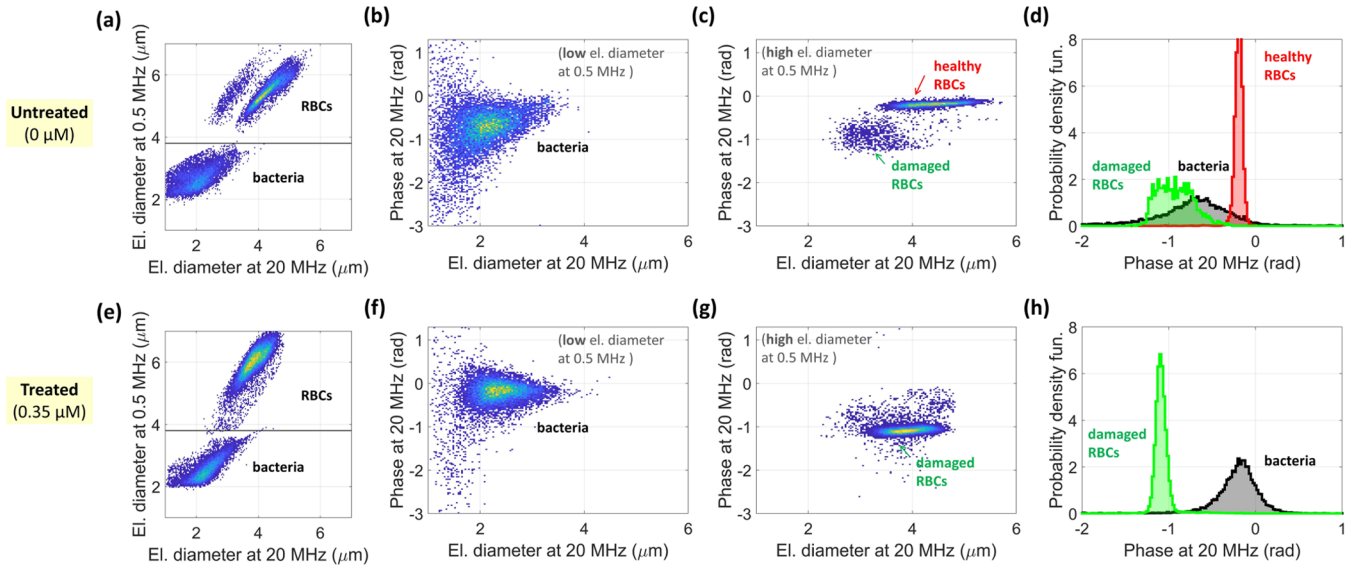

Figure 4. Results of impedance-based analysis of mixed samples (i.e., containing both *B. megaterium* cells and RBCs): (a−d) untreated sample (0 μM) and (e−h) treated sample (0.35 μM). (a, e) Density plot of the electrical diameter at 0.5 MHz against the electrical diameter at 20 MHz, with highlight of relevant subpopulations. The gating line is also shown (electrical diameter at 0.5 MHz equal to 3.8 μm). (b, f) [resp. (c, g)] Density plot of the phase at 20 MHz against the electrical diameter at 20 MHz for the bacterial cells [resp. for the RBCs]. (d, h) Empirical probability density function of the phase at 20 MHz, for each subpopulation.

hemoglobin release (eq 3) for the tested peptide concentrations along with the relevant fit (parameter values: K = 0.15 ± 0.02 μM, n = 1.5 ± 0.3). The results indicate that RBCs are susceptible to the DNS-PMAP23 peptide, in agreement with previous reports.[14] Figure 3c also shows the normalized fraction of subpopulation L (eq 5) and the corresponding fit (parameter values: K = 0.17 ± 0.04 μM, n = 2.5 ± 1.4).

The hemoglobin release caused by the incubation of RBCs with DNS-PMAP23 at increasing concentrations is reflected in a progressive increase of subpopulation L, with similar values of fitted parameters. These results suggest that the latter subpopulation represents damaged RBCs, whereas subpopulation H, which is dominant at low peptide concentration, represents healthy RBCs.

Characterization of a Mixed Sample of *B. megaterium* cells and RBCs. Figure 4a shows the density plot of the electrical diameter at 0.5 MHz against the electrical diameter at 20 MHz for the untreated (i.e., no peptide incubation) mixed sample. Three subpopulations are found. Based on the analysis of the separate samples (Figures 2a and 3a), the subpopulation with lower electrical diameter at 0.5 MHz (i.e., <3.8 μm) corresponds to bacterial cells, whereas the two subpopulations with higher electrical diameter at 0.5 MHz (i.e., >3.8 μm) correspond to RBCs. This criterion has been used to study the two cell types separately in subsequent analyses. Figure 4b,c shows the density plot of the phase at 20 MHz against the electrical diameter at 20 MHz for the bacterial cells and for the RBCs, respectively. Of the two RBC subpopulations, the main one shows higher values of both the electrical diameter and the phase (i.e., −0.2 rad median phase value against −0.9 rad). In agreement with the analysis of the RBC sample previously reported, the main RBC subpopulation corresponds to healthy RBCs (subpopulation H), whereas the minor subpopulation represents damaged RBCs (subpopulation L). Figure 4d shows the empirical probability density function of the phase at 20 MHz for the three subpopulations.

The analysis of the treated (i.e., peptide incubation at 0.35 μM) mixed sample is reported in Figure 4e−h. Two subpopulations appear in the density plot of the electrical diameter at 0.5 MHz against the electrical diameter at 20 MHz (Figure 4e), which are identified as bacteria (electrical diameter at 0.5 MHz < 3.8 μm) and RBCs (electrical diameter at 0.5 MHz > 3.8 μm). The separate density plots of the phase at 20 MHz against the electrical diameter at 20 MHz for the bacterial cells and for the RBCs are shown in Figure 4f,g, respectively, while the empirical probability density function of the phase at 20 MHz is reported in Figure 4h, for both subpopulations. Peptide exposure induces an increase in the median phase of bacterial cells (i.e., from −0.7 to −0.2 rad). A similar trend was obtained with the sample containing bacterial cells alone. Furthermore, the RBC subpopulation in the treated sample exhibits the reduced phase typical of the damaged RBCs.

DISCUSSION

AMPs hold promises to fight AMR. However, AMP development requires AST methods that are fast (minutes) and able to assess AMP activity and cytotoxicity in the presence of both bacterial and eukaryotic cell types, with single-cell sensitivity. Among the microfluidic technologies that are being explored in AST research,[61,62] single-cell impedance cytometry seems particularly suited to meet these requirements.[23]

Impedance cytometry provides single-cell electrical fingerprints that convey information about intrinsic cell properties. At a low frequency, cells with intact membrane behave as insulating particles and the impedance signal is proportional to the cell volume. Changes in membrane capacitance are observed in the mid-frequency range, whereas changes in cytoplasmic properties affect the high-frequency part of the spectrum.[22,23,63] As discussed in the introduction, AMP effects in principle could affect all of these properties.

In this work, the frequency-dependent cell electrical phenotypes were quantified in terms of the electrical diameter

https://doi.org/10.1021/acssensors.3c00256
ACS Sens. 2023, 8, 2572−2582

and electrical phase, which are common metrics for impedance-based cell characterization. The electrical diameter was recently used to characterize the response of susceptible bacteria to traditional antibiotics. For β-lactam-type antibiotics, which mainly work by inhibiting cell wall biosynthesis, either an increase or a reduction of the low-frequency electrical diameter was reported, depending on the bacterial type (Gram-negative *vs* Gram-positive).[22,37] For colistin, which affects membrane permeability in Gram-negative bacteria, a reduction in the electrical diameter of *Klebsiella pneumoniae* was found.[22] Broadly speaking, the mode of action of DNS-PMAP23 (membrane perturbation) is analogous to that of colistin, even though the latter targets lipopolysaccharides,[64] while the former does not interact with them specifically.[43] Our results (Figure 2a) did not show specific alterations of the electrical diameter of *B. megaterium* (Gram-positive) upon exposure to different peptide concentrations. These findings were in agreement with SEM images of treated and untreated cells (Figure S3). On the other hand, upon peptide exposure, we found significant variations of the high-frequency phase of *B. megaterium* (Figure 2b,c). Specifically, the phases at 11 and 20 MHz increase with increasing peptide concentration. A similar increase in the high-frequency (40 MHz) phase was recently reported for *Staphylococcus aureus* (Gram-positive) exposed to Cefoxitin (β-lactam-type antibiotic).[22] The electrical phase was also used in the literature to monitor bacterial inactivation[35,36] and bacterial spore germination.[65]

To test the sensitivity of the system, we performed an additional experiment with *E. coli* cells whose size is significantly smaller than that of *B. megaterium* cells. The relevant results are reported in Figure S4. The system was able to detect *E. coli* cells. No significant change of the electrical size at 0.5 MHz was found after 30 min incubation with DNS-PMAP23 at 2.5 μM. A change of the phase at 20 MHz was detected. This encourages the use of the high-frequency phase to quantify the effect of peptide treatment also on *E. coli*, which will be the subject of further investigation.

Impedance-based characterization of RBCs revealed the presence of two subpopulations (Figure 3a,b), which were identified as healthy RBCs and damaged RBCs. Their electrical diameters were similar irrespective of the frequency (in fact, the electrical diameter of the damaged RBC subpopulation was slightly smaller than that of the healthy subpopulation at 20 MHz). Their phases were similar at 0.5 MHz (and slightly lower than that of the reference beads), whereas the phase of the damaged subpopulation showed a significant reduction at 11 and 20 MHz. By referring to the single-shell model—which is commonly used for the interpretation of the RBC impedance spectrum[22,55]—the behavior of damaged RBCs compared to healthy RBCs is compatible with an increase in the membrane conductivity (due to pore formation) and an increase of the intracellular conductivity and permittivity (due to hemoglobin release and cytoplasm replacement by suspension medium) (cf. Figure S5). These structural modifications are reflected in an altered optical behavior (damaged RBCs turned out to be invisible with the present imaging setup).

Based on the electrical characterization, we were able to build the DNS-PMAP23 antibacterial activity and RBC cytotoxicity curves. A general agreement with the activity and cytotoxicity curves obtained with the reference methods was found (Figures 2e and 3c). The RBC cytotoxicity assays based on impedance or hemoglobin release showed comparable behaviors (Figure 3c). Regarding the antibacterial activity, the Hill coefficient provided by the standard approach was noticeably higher than that of the impedance-based approach (i.e., 2.7 vs 0.4). A possible explanation for this observation is that the two approaches are measuring different effects. In fact, the standard assay accounts for biological cell changes (bacterial killing), whereas the impedance-based approach accounts for biophysical cell changes (structural modifications). Since, as discussed above, the high-frequency phase is influenced mainly by the cytosolic properties, the impedance signal could reflect peptide accumulation inside the killed bacterial cells, which is known to take place following membrane perturbation.[17,19,41−43] The observed increase of the high-frequency phase even at AMP concentrations, where bacterial killing by membrane perturbation is essentially complete, could be explained by a progressive peptide accumulation in the cytosol. It is currently debated whether peptide entry into the cytosol is simply a consequence of membrane disruption, or if it is required for bacterial killing.[17,43] The difference observed between the antibacterial curves obtained by measuring CFUs and by impedance cytometry might support the former hypothesis. This aspect is currently being investigated further.

The impedance measurements were performed right after peptide incubation, without further preparation or washing steps, except for the addition of the calibration beads. For each experimental condition, several thousands of cells were measured (~5 min acquisition time) and analyzed (~5 min processing time). Compared to the long times (overnight incubation) required by the CFU-count-based activity assay, the rapidity of the impedance-based assay is a major advantage. The timeframe of the standard cytotoxicity assay based on hemoglobin release is not critical, since it is essentially set by the 10 min centrifugation step. However, the standard cytotoxicity assay lacks single-cell sensitivity and cannot provide information on sample heterogeneity (i.e., the presence of RBC subpopulations).

Whereas substantially different assays are traditionally used for activity testing (i.e., CFU-count-based bacterial killing) and for cytotoxicity testing (i.e., absorbance-based RBC hemoglobin release), microfluidic impedance cytometry can serve both purposes. The technique also has the potential for simultaneous AST of bacteria and determination of toxicity to host cells, as shown by the reported proof-of-concept experiment with a mixture of *B. megaterium* and RBCs (Figure 4). A sample where host cells and pathogens coexist mimics an infection in vivo significantly better than the separate assays normally employed to assess AMP selectivity.[14,15] The potential of impedance cytometry to analyze samples in biofluids such as whole blood[66] and urine[67] is also attractive. In view of its rapidity and versatility, impedance cytometry is uniquely posed to develop next-generation AST approaches and holds promises for AMP screening and optimization.

CONCLUSIONS

In this work, we presented the application of single-cell microfluidic impedance cytometry to assess the susceptibility of bacterial cells (*B. megaterium* cells) and host cells (RBCs) to a representative antimicrobial peptide (DNS-PMAP23). Impedance cytometry turned out to be an effective way for rapid assessment of both antimicrobial activity and RBC cytotoxicity, as confirmed by comparison with standard bacterial killing assays and hemolytic activity assays. Overall, the main merits of the proposed technique with respect to

https://doi.org/10.1021/acssensors.3c00256
ACS Sens. 2023, 8, 2572−2582

traditional approaches are as follows: (i) the suitability to both bacterial and host cells (even in the same sample), (ii) the rapidity of the analysis (thousands of cells in a few minutes), and (iii) the single-cell sensitivity (which enables subpopulation analysis). Further studies will focus on the characterization of mixed samples with bacteria and RBCs at different relative concentrations to shed light into possible interactions and peptide sequestration mechanisms.

■ ASSOCIATED CONTENT

Supporting Information

The Supporting Information is available free of charge at https://pubs.acs.org/doi/10.1021/acssensors.3c00256.

Summary table of impedance-based systems for susceptibility assessment of bacteria at the single-cell level; details of the microfluidic impedance chip; bipolar Gaussian template; SEM images of *B. megaterium* cells; impedance-based analysis of *E. coli* cells; simulated impedance spectra; and simulation parameters table (PDF)

■ AUTHOR INFORMATION

Corresponding Authors

Lorenzo Stella − *Department of Chemical Science and Technologies, University of Rome Tor Vergata, 00133 Rome, Italy;* orcid.org/0000-0002-5489-7381; Email: stella@stc.uniroma2.it

Federica Caselli − *Department of Civil Engineering and Computer Science, University of Rome Tor Vergata, 00133 Rome, Italy;* orcid.org/0000-0001-6663-8603; Email: caselli@ing.uniroma2.it

Authors

Cassandra Troiano − *Department of Chemical Science and Technologies, University of Rome Tor Vergata, 00133 Rome, Italy*

Adele De Ninno − *Institute for Photonics and Nanotechnologies, Italian National Research Council, 00133 Rome, Italy*

Bruno Casciaro − *Laboratory affiliated to Pasteur Italia-Fondazione Cenci Bolognetti, Department of Biochemical Sciences "A. Rossi Fanelli", Sapienza University of Rome, 00185 Rome, Italy*

Francesco Riccitelli − *Department of Chemical Science and Technologies, University of Rome Tor Vergata, 00133 Rome, Italy*

Yoonkyung Park − *Department of Biomedical Science, College of Natural science, Chosun University, Gwangju 61452, Republic of Korea;* orcid.org/0000-0002-8717-3080

Luca Businaro − *Institute for Photonics and Nanotechnologies, Italian National Research Council, 00133 Rome, Italy*

Renato Massoud − *Department of Experimental Medicine, University of Rome Tor Vergata, 00133 Rome, Italy*

Maria Luisa Mangoni − *Laboratory affiliated to Pasteur Italia-Fondazione Cenci Bolognetti, Department of Biochemical Sciences "A. Rossi Fanelli", Sapienza University of Rome, 00185 Rome, Italy;* orcid.org/0000-0002-5991-5868

Paolo Bisegna − *Department of Civil Engineering and Computer Science, University of Rome Tor Vergata, 00133 Rome, Italy*

Complete contact information is available at: https://pubs.acs.org/10.1021/acssensors.3c00256

Author Contributions

[▽]C.T. and A.D.N. contributed equally to this work. Conceptualization: L.S., F.C., P.B.; methodology: L.S., F.C., P.B., M.L.M., C.T., A.D.N., B.C., L.B.; software: F.C., P.B.; formal analysis: F.C., C.T., L.S., P.B.; investigation: C.T., A.D.N., F.C., B.C., R.M., F.R., L.B.; resources: A.D.N., F.C., L.S., Y.K.P., M.L.M., R.M.; writing—original draft: F.C., L.S., C.T.; writing—review and editing: all authors; visualization: F.C., C.T., B.C., L.S.; supervision: L.S., M.L.M.; project administration: F.C., L.S.; funding acquisition: L.S., F.C., A.D.N., Y.K.P.

Notes

The authors declare no competing financial interest.

■ ACKNOWLEDGMENTS

This work was supported by the Regione Lazio (Research Groups 2020 Programme, POR FESR Lazio 2014-2020, E85F21002390002, to F.C. and A.D.N.), the Italian Ministry of University and Research (PRIN 2020833Y75, to L.S.), and the National Research Foundation (NRF) of Korea (No. NRF-2022M3A9H5096106, to Y.K.P.).

■ REFERENCES

(1) Laxminarayan, R. The Overlooked Pandemic of Antimicrobial Resistance. *Lancet* **2022**, *399*, 606−607.

(2) Murray, C. J. L.; Ikuta, K. S.; Sharara, F.; Swetschinski, L.; Aguilar, G. R.; Gray, A.; Han, C.; Bisignano, C.; Rao, P.; Wool, E.; Johnson, S. C.; Browne, A. J.; Chipeta, M. G.; Fell, F.; Hackett, S.; Haines-Woodhouse, G.; Hamadani, B. H. K.; Kumaran, E. A. P.; McManigal, B.; Agarwal, R.; Akech, S.; Albertson, S.; Amuasi, J.; Andrews, J.; Aravkin, A.; Ashley, E.; Bailey, F.; Baker, S.; Basnyat, B.; Bekker, A.; Bender, R.; Bethou, A.; Bielicki, J.; Boonkasidecha, S.; Bukosia, J.; Carvalheiro, C.; Castañeda-Orjuela, C.; Chansamouth, V.; Chaurasia, S.; Chiurchiù, S.; Chowdhury, F.; Cook, A. J.; Cooper, B.; Cressey, T. R.; Criollo-Mora, E.; Cunningham, M.; Darboe, S.; Day, N. P. J.; De Luca, M.; Dokova, K.; Dramowski, A.; Dunachie, S. J.; Eckmanns, T.; Eibach, D.; Emami, A.; Feasey, N.; Fisher-Pearson, N.; Forrest, K.; Garrett, D.; Gastmeier, P.; Giref, A. Z.; Greer, R. C.; Gupta, V.; Haller, S.; Haselbeck, A.; Hay, S. I.; Holm, M.; Hopkins, S.; Iregbu, K. C.; Jacobs, J.; Jarovsky, D.; Javanmardi, F.; Khorana, M.; Kissoon, N.; Kobeissi, E.; Kostyanev, T.; Krapp, F.; Krumkamp, R.; Kumar, A.; Kyu, H. H.; Lim, C.; Limmathurotsakul, D.; Loftus, M. J.; Lunn, M.; Ma, J.; Mturi, N.; Munera-Huertas, T.; Musicha, P.; Mussi-Pinhata, M. M.; Nakamura, T.; Nanavati, R.; Nangia, S.; Newton, P.; Ngoun, C.; Novotney, A.; Nwakanma, D.; Obiero, C. W.; Olivas-Martinez, A.; Olliaro, P.; Ooko, E.; Ortiz-Brizuela, E.; Peleg, A. Y.; Perrone, C.; Plakkal, N.; Ponce-de-Leon, A.; Raad, M.; Ramdin, T.; Riddell, A.; Roberts, T.; Robotham, J. V.; Roca, A.; Rudd, K. E.; Russell, N.; Schnall, J.; Scott, J. A. G.; Shivamallappa, M.; Sifuentes-Osornio, J.; Steenkeste, N.; Stewardson, A. J.; Stoeva, T.; Tasak, N.; Thaiprakong, A.; Thwaites, G.; Turner, C.; Turner, P.; van Doorn, H. R.; Velaphi, S.; Vongpradith, A.; Vu, H.; Walsh, T.; Waner, S.; Wangrangsimakul, T.; Wozniak, T.; Zheng, P.; Sartorius, B.; Lopez, A. D.; Stergachis, A.; Moore, C.; Dolecek, C.; Naghavi, M.; et al. Global Burden of Bacterial Antimicrobial Resistance in 2019: A Systematic Analysis. *Lancet* **2022**, *399*, 629−655.

(3) Teillant, A.; Gandra, S.; Barter, D.; Morgan, D. J.; Laxminarayan, R. Potential Burden of Antibiotic Resistance on Surgery and Cancer Chemotherapy Antibiotic Prophylaxis in the USA: A Literature Review and Modelling Study. *Lancet Infect. Dis.* **2015**, *15*, 1429−1437.

(4) Plackett, B. Why Big Pharma Has Abandoned Antibiotics. *Nature* **2020**, *586*, S50−S52.

(5) Magana, M.; Pushpanathan, M.; Santos, A. L.; Leanse, L.; Fernandez, M.; Ioannidis, A.; Giulianotti, M. A.; Apidianakis, Y.;

Bradfute, S.; Ferguson, A. L.; Cherkasov, A.; Seleem, M. N.; Pinilla, C.; de la Fuente-Nunez, C.; Lazaridis, T.; Dai, T.; Houghten, R. A.; Hancock, R. E. W.; Tegos, G. P. The Value of Antimicrobial Peptides in the Age of Resistance. *Lancet Infect. Dis.* **2020**, *20*, e216−2230.
(6) Lazzaro, B. P.; Zasloff, M.; Rolff, J. Antimicrobial Peptides: Application Informed by Evolution. *Science* **2020**, *368*, No. eaau5480.
(7) Matsuzaki, K. Membrane Permeabilization Mechanisms. In *Advances in Experimental Medicine and Biology*; Springer, 2019; Vol. *1117*.
(8) Roversi, D.; Luca, V.; Aureli, S.; Park, Y.; Mangoni, M. L.; Stella, L. How Many Antimicrobial Peptide Molecules Kill a Bacterium? The Case of PMAP-23. *ACS Chem. Biol.* **2014**, *9*, 2003−2007.
(9) Spohn, R.; Daruka, L.; Lázár, V.; Martins, A.; Vidovics, F.; Grézal, G.; Méhi, O.; Kintses, B.; Számel, M.; Jangir, P. K.; Csörgő, B.; Györkei, Á.; Bódi, Z.; Faragó, A.; Bodai, L.; Földesi, I.; Kata, D.; Maróti, G.; Pap, B.; Wirth, R.; Papp, B.; Pál, C. Integrated Evolutionary Analysis Reveals Antimicrobial Peptides with Limited Resistance. *Nat. Commun.* **2019**, *10*, No. 4538.
(10) Madhusoodanan, J. Innovative Tools Take Aim at Antibiotic-Resistant Microbes. *Nature* **2021**, *596*, 611−613.
(11) van Belkum, A.; Burnham, C. A. D.; Rossen, J. W. A.; Mallard, F.; Rochas, O.; Dunne, W. M. Innovative and Rapid Antimicrobial Susceptibility Testing Systems. *Nat. Rev. Microbiol.* **2020**, *18*, 299−311.
(12) Meurer, M.; O'Neil, D. A.; Lovie, E.; Simpson, L.; Torres, M. D. T.; De La Fuente-Nunez, C.; Angeles-Boza, A. M.; Kleinsorgen, C.; Mercer, D. K.; Von Köckritz-Blickwede, M. Antimicrobial Susceptibility Testing of Antimicrobial Peptides Requires New and Standardized Testing Structures. *ACS Infect. Dis.* **2021**, *7*, 2205−2208.
(13) Bobone, S.; Stella, L. Selectivity of Antimicrobial Peptides: A Complex Interplay of Multiple Equilibria. In *Advances in Experimental Medicine and Biology*; Springer, 2019; Vol. *1117*, pp 175−214.
(14) Savini, F.; Luca, V.; Bocedi, A.; Massoud, R.; Park, Y.; Mangoni, M. L.; Stella, L. Cell-Density Dependence of Host-Defense Peptide Activity and Selectivity in the Presence of Host Cells. *ACS Chem. Biol.* **2017**, *12*, 52−56.
(15) Loffredo, M. R.; Savini, F.; Bobone, S.; Casciaro, B.; Franzyk, H.; Mangoni, M. L.; Stella, L. Inoculum Effect of Antimicrobial Peptides. *Proc. Natl. Acad. Sci. U.S.A.* **2021**, *118*, No. e2014364118.
(16) Starr, C. G.; He, J.; Wimley, W. C. Host Cell Interactions Are a Significant Barrier to the Clinical Utility of Peptide Antibiotics. *ACS Chem. Biol.* **2016**, *11*, 3391−3399.
(17) Semeraro, E. F.; Marx, L.; Mandl, J.; Letofsky-Papst, I.; Mayrhofer, C.; Frewein, M. P. K.; Scott, H. L.; Prévost, S.; Bergler, H.; Lohner, K.; Pabst, G. Lactoferricins Impair the Cytosolic Membrane of Escherichia Coli within a Few Seconds and Accumulate inside the Cell. *eLife* **2022**, *11*, No. e72850.
(18) Cama, J.; Pagliara, S. Microfluidic Single-Cell Phenotyping of the Activity of Peptide-Based Antimicrobials. In *Methods in Molecular Biology*; Springer, 2021; Vol. *2208*, pp 237−253.
(19) Snoussi, M.; Talledo, J. P.; Del Rosario, N. A.; Mohammadi, S.; Ha, B. Y.; Košmrlj, A.; Taheri-Araghi, S. Heterogeneous Absorption of Antimicrobial Peptide LL37 in Escherichia Coli Cells Enhances Population Survivability. *eLife* **2018**, *7*, No. e38174.
(20) Jepson, A. K.; Schwarz-Linek, J.; Ryan, L.; Ryadnov, M. G.; Poon, W. C. K. What Is the "Minimum Inhibitory Concentration" (MIC) of Pexiganan Acting on Escherichia Coli?—A Cautionary Case Study. In *Advances in Experimental Medicine and Biology*; Springer, 2016; Vol. *915*, pp 33−48.
(21) Bamford, R. A.; Smith, A.; Metz, J.; Glover, G.; Titball, R. W.; Pagliara, S. Investigating the Physiology of Viable but Non-Culturable Bacteria by Microfluidics and Time-Lapse Microscopy. *BMC Biol.* **2017**, *15*, No. 121.
(22) Spencer, D. C.; Paton, T. F.; Mulroney, K. T.; Inglis, T. J. J.; Sutton, J. M.; Morgan, H. A Fast Impedance-Based Antimicrobial Susceptibility Test. *Nat. Commun.* **2020**, *11*, No. 5328.
(23) Honrado, C.; Bisegna, P.; Swami, N. S.; Caselli, F. Single-Cell Microfluidic Impedance Cytometry: From Raw Signals to Cell Phenotypes Using Data Analytics. *Lab Chip* **2021**, *21*, 22−54.
(24) Daguerre, H.; Solsona, M.; Cottet, J.; Gauthier, M.; Renaud, P.; Bolopion, A. Positional Dependence of Particles and Cells in Microfluidic Electrical Impedance Flow Cytometry: Origin, Challenges and Opportunities. *Lab Chip* **2020**, *20*, 3665−3689.
(25) Tang, T.; Liu, X.; Kiya, R.; Shen, Y.; Yuan, Y.; Zhang, T.; Suzuki, K.; Tanaka, Y.; Li, M.; Hosokawa, Y.; Yalikun, Y. Microscopic Impedance Cytometry for Quantifying Single Cell Shape. *Biosens. Bioelectron.* **2021**, *193*, No. 113521.
(26) de Bruijn, D. S.; ter Braak, P. M.; van de Waal, D. B.; Olthuis, W.; van den Berg, A. Coccolithophore Calcification Studied by Single-Cell Impedance Cytometry: Towards Single-Cell PIC:POC Measurements. *Biosens. Bioelectron.* **2021**, *173*, No. 112808.
(27) Gökçe, F.; Ravaynia, P. S.; Modena, M. M.; Hierlemann, A. What Is the Future of Electrical Impedance Spectroscopy in Flow Cytometry. *Biomicrofluidics* **2021**, *15*, No. 061302.
(28) Petchakup, C.; Tay, H. M.; Yeap, W. H.; Dalan, R.; Wong, S. C.; Li, K. H. H.; Hou, H. W. Label-Free Leukocyte Sorting and Impedance-Based Profiling for Diabetes Testing. *Biosens. Bioelectron.* **2018**, *118*, 195−203.
(29) Kruit, S. A.; de Bruijn, D. S.; Broekhuijse, M. L. W. J.; Olthuis, W.; Segerink, L. I. Label-Free Microfluidic Impedance Cytometry for Acrosome Integrity Assessment of Boar Spermatozoa. *Biosensors* **2022**, *12*, No. 679.
(30) Wang, M.; Tan, H.; Li, Y.; Chen, X.; Chen, D.; Wang, J.; Chen, J. Toward Five-Part Differential of Leukocytes Based on Electrical Impedances of Single Cells and Neural Network. *Cytometry, Part A* **2022**, *103*, 439−446.
(31) De Ninno, A.; Reale, R.; Giovinazzo, A.; Bertani, F. R.; Businaro, L.; Bisegna, P.; Matteucci, C.; Caselli, F. High-Throughput Label-Free Characterization of Viable, Necrotic and Apoptotic Human Lymphoma Cells in a Coplanar-Electrode Microfluidic Impedance Chip. *Biosens. Bioelectron.* **2020**, *150*, No. 111887.
(32) Zhong, J.; Yang, D.; Zhou, Y.; Liang, M.; Ai, Y. Multi-Frequency Single Cell Electrical Impedance Measurement for Label-Free Cell Viability Analysis. *Analyst* **2021**, *146*, 1848−1858.
(33) Honrado, C.; Adair, S. J.; Moore, J. H.; Salahi, A.; Bauer, T. W.; Swami, N. S. Apoptotic Bodies in the Pancreatic Tumor Cell Culture Media Enable Label-Free Drug Sensitivity Assessment by Impedance Cytometry. *Adv. Biol.* **2021**, *5*, No. 2100438.
(34) Honrado, C.; Salahi, A.; Adair, S. J.; Moore, J. H.; Bauer, T. W.; Swami, N. S. Automated Biophysical Classification of Apoptotic Pancreatic Cancer Cell Subpopulations by Using Machine Learning Approaches with Impedance Cytometry. *Lab Chip* **2022**, *22*, 3708−3720.
(35) David, F.; Hebeisen, M.; Schade, G.; Franco-Lara, E.; di Berardino, M. Viability and Membrane Potential Analysis of Bacillus Megaterium Cells by Impedance Flow Cytometry. *Biotechnol. Bioeng.* **2012**, *109*, 483−492.
(36) Bertelsen, C. V.; Franco, J. C.; Skands, G. E.; Dimaki, M.; Svendsen, W. E. Investigating the Use of Impedance Flow Cytometry for Classifying the Viability State of E. Coli. *Sensors* **2020**, *20*, No. 6339.
(37) Tang, T.; Liu, X.; Yuan, Y.; Kiya, R.; Zhang, T.; Yang, Y.; Suetsugu, S.; Yamazaki, Y.; Ota, N.; Yamamoto, K.; Kamikubo, H.; Tanaka, Y.; Li, M.; Hosokawa, Y.; Yalikun, Y. Machine Learning-Based Impedance System for Real-Time Recognition of Antibiotic-Susceptible Bacteria with Parallel Cytometry. *Sens. Actuators, B* **2023**, *374*, No. 132698.
(38) Tang, T.; Liu, X.; Yuan, Y.; Zhang, T.; Kiya, R.; Yang, Y.; Yamazaki, Y.; Kamikubo, H.; Tanaka, Y.; Li, M.; Hosokawa, Y.; Yalikun, Y. Parallel Impedance Cytometry for Real-Time Screening of Bacterial Single Cells from Nano- to Microscale. *ACS Sens.* **2022**, *7*, 3700−3709.
(39) Hartmann, M.; Berditsch, M.; Hawecker, J.; Ardakani, M. F.; Gerthsen, D.; Ulrich, A. S. Damage of the Bacterial Cell Envelope by Antimicrobial Peptides Gramicidin S and PGLa as Revealed by Transmission and Scanning Electron Microscopy. *Antimicrob. Agents Chemother.* **2010**, *54*, 3132−3142.

https://doi.org/10.1021/acssensors.3c00256
ACS Sens. 2023, 8, 2572−2582

(40) Marcellini, L.; Giammatteo, M.; Aimola, P.; Mangoni, M. L. Fluorescence and Electron Microscopy Methods for Exploring Antimicrobial Peptides Mode(s) of Action. *Methods Mol. Biol.* **2010**, *618*, 249−266.
(41) Kaji, T.; Yano, Y.; Matsuzaki, K. In-Cell FRET Indicates Magainin Peptide Induced Permeabilization of Bacterial Cell Membranes at Lower Peptide-to-Lipid Ratios Relevant to Liposomal Studies. *ACS Infect. Dis.* **2021**, *7*, 2941−2945.
(42) Wu, F.; Tan, C. Dead Bacterial Absorption of Antimicrobial Peptides Underlies Collective Tolerance. *J. R. Soc., Interface* **2019**, *16*, No. 20180701.
(43) Savini, F.; Loffredo, M. R.; Troiano, C.; Bobone, S.; Malanovic, N.; Eichmann, T. O.; Caprio, L.; Canale, V. C.; Park, Y.; Mangoni, M. L.; Stella, L. Binding of an Antimicrobial Peptide to Bacterial Cells: Interaction with Different Species, Strains and Cellular Components. *Biochim. Biophys. Acta, Biomembr.* **2020**, *1862*, No. 183291.
(44) Zhu, Y.; Mohapatra, S.; Weisshaar, J. C. Rigidification of the Escherichia Coli Cytoplasm by the Human Antimicrobial Peptide LL-37 Revealed by Superresolution Fluorescence Microscopy. *Proc. Natl. Acad. Sci. U.S.A.* **2019**, *116*, 1017−1026.
(45) Zhu, Y.; Liu, L.; Mustafi, M.; Rank, L. A.; Gellman, S. H.; Weisshaar, J. C. Local Rigidification and Possible Coacervation of the Escherichia Coli DNA by Cationic Nylon-3 Polymers. *Biophys. J.* **2021**, *120*, 5243−5254.
(46) Zanetti, M.; Storici, P.; Tossi, A.; Scocchi, M.; Gennaro, R. Molecular Cloning and Chemical Synthesis of a Novel Antibacterial Peptide Derived from Pig Myeloid Cells. *J. Biol. Chem.* **1994**, *269*, 7855−7858.
(47) Lee, D. G.; Kim, D. H.; Park, Y.; Kim, H. K.; Kim, H. N.; Shin, Y. K.; Choi, C. H.; Hahm, K. S. Fungicidal Effect of Antimicrobial Peptide, PMAP-23, Isolated from Porcine Myeloid against Candida Albicans. *Biochem. Biophys. Res. Commun.* **2001**, *282*, 570−574.
(48) Park, Y.; Jang, S. H.; Lee, D. G.; Hahm, K. S. Antinematodal Effect of Antimicrobial Peptide, PMAP-23, Isolated from Porcine Myeloid against Caenorhabditis Elegans. *J. Pept. Sci.* **2004**, *10*, 304−311.
(49) Orioni, B.; Bocchinfuso, G.; Kim, J. Y.; Palleschi, A.; Grande, G.; Bobone, S.; Park, Y.; Kim, J. I.; Hahm, K. S.; Stella, L. Membrane Perturbation by the Antimicrobial Peptide PMAP-23: A Fluorescence and Molecular Dynamics Study. *Biochim. Biophys. Acta, Biomembr.* **2009**, *1788*, 1523−1533.
(50) Bocchinfuso, G.; Palleschi, A.; Orioni, B.; Grande, G.; Formaggio, F.; Toniolo, C.; Park, Y.; Hahm, K. S.; Stella, L. Different Mechanisms of Action of Antimicrobial Peptides: Insights from Fluorescence Spectroscopy Experiments and Molecular Dynamics Simulations. *J. Pept. Sci.* **2009**, *15*, 550−558.
(51) Caselli, F.; De Ninno, A.; Reale, R.; Businaro, L.; Bisegna, P. A Bayesian Approach for Coincidence Resolution in Microfluidic Impedance Cytometry. *IEEE Trans. Biomed. Eng.* **2021**, *68*, 340−349.
(52) Reale, R.; De Ninno, A.; Businaro, L.; Bisegna, P.; Caselli, F. High-Throughput Electrical Position Detection of Single Flowing Particles/Cells with Non-Spherical Shape. *Lab Chip* **2019**, *19*, 1818−1827.
(53) Xie, X.; Gong, M.; Zhang, Z.; Dou, X.; Zhou, W.; Li, J.; Zhu, M.; Du, Y.; Xu, X. Optimization of an Electrical Impedance Flow Cytometry System and Analysis of Submicron Particles and Bacteria. *Sens. Actuators, B* **2022**, *360*, No. 131432.
(54) Liu, X.; Tang, T.; Yi, P. W.; Yuan, Y.; Lei, C.; Li, M.; Tanaka, Y.; Hosokawa, Y.; Yalikun, Y. Identification of Single Yeast Budding Using Impedance Cytometry with a Narrow Electrode Span. *Sensors* **2022**, *22*, No. 7743.
(55) Salahi, A.; Honrado, C.; Rane, A.; Caselli, F.; Swami, N. S. Modified Red Blood Cells as Multimodal Standards for Benchmarking Single-Cell Cytometry and Separation Based on Electrical Physiology. *Anal. Chem.* **2022**, *94*, 2865−2872.
(56) Errico, V.; De Ninno, A.; Bertani, F. R.; Businaro, L.; Bisegna, P.; Caselli, F. Mitigating Positional Dependence in Coplanar Electrode Coulter-Type Microfluidic Devices. *Sens. Actuators, B* **2017**, *247*, 580−586.
(57) Honrado, C.; McGrath, J. S.; Reale, R.; Bisegna, P.; Swami, N. S.; Caselli, F. A Neural Network Approach for Real-Time Particle/Cell Characterization in Microfluidic Impedance Cytometry. *Anal. Bioanal. Chem.* **2020**, *412*, 3835−3845.
(58) Caselli, F.; Reale, R.; De Ninno, A.; Spencer, D.; Morgan, H.; Bisegna, P. Deciphering Impedance Cytometry Signals with Neural Networks. *Lab Chip* **2022**, *22*, 1714−1722.
(59) D'Orazio, M.; Reale, R.; De Ninno, A.; Brighetti, M. A.; Mencattini, A.; Businaro, L.; Martinelli, E.; Bisegna, P.; Travaglini, A.; Caselli, F. Electro-Optical Classification of Pollen Grains via Microfluidics and Machine Learning. *IEEE Trans. Biomed. Eng.* **2021**, *69*, 921−931.
(60) Reale, R.; De Ninno, A.; Nepi, T.; Bisegna, P.; Caselli, F. Extensional-Flow Impedance Cytometer for Contactless and Optics-Free Erythrocyte Deformability Analysis. *IEEE Trans. Biomed. Eng.* **2022**, 565−572.
(61) Postek, W.; Pacocha, N.; Garstecki, P. Microfluidics for Antibiotic Susceptibility Testing. *Lab Chip* **2022**, *22*, 3637−3662.
(62) Qin, N.; Zhao, P.; Ho, E. A.; Xin, G.; Ren, C. L. Microfluidic Technology for Antibacterial Resistance Study and Antibiotic Susceptibility Testing: Review and Perspective. *ACS Sens.* **2021**, *6*, 3−21.
(63) Gawad, S.; Cheung, K.; Seger, U.; Bertsch, A.; Renaud, P. Dielectric Spectroscopy in a Micromachined Flow Cytometer: Theoretical and Practical Considerations. *Lab Chip* **2004**, *4*, 241−251.
(64) Sabnis, A.; Hagart, K. L. H.; Klöckner, A.; Becce, M.; Evans, L. E.; Furniss, R. C. D.; Mavridou, D. A. I.; Murphy, R.; Stevens, M. M.; Davies, J. C.; Larrouy-Maumus, G. J.; Clarke, T. B.; Edwards, A. M. Colistin Kills Bacteria by Targeting Lipopolysaccharide in the Cytoplasmic Membrane. *eLife* **2021**, *10*, No. e65836.
(65) Moore, J. H.; Honrado, C.; Stagnaro, V.; Kolling, G.; Warren, C. A.; Swami, N. S. Rapid in Vitro Assessment of Clostridioides Difficile Inhibition by Probiotics Using Dielectrophoresis to Quantify Cell Structure Alterations. *ACS Infect. Dis.* **2020**, *6*, 1000−1007.
(66) Hassan, U.; Reddy, B.; Damhorst, G.; Sonoiki, O.; Ghonge, T.; Yang, C.; Bashir, R. A Microfluidic Biochip for Complete Blood Cell Counts at the Point-of-Care. *Technology* **2015**, *03*, 201−213.
(67) Petchakup, C.; Tay, H. M.; Hon, P. Y.; De, P. P.; Yeo, T. W.; Holden, K. H.; Li, S. V.; H, W. H. In *Label-Free and Rapid Detection of Urinary Tract Infection Using Impedance Cytometry*; 26th International Conference on Miniaturized Systems for Chemistry and Life Sciences (MicroTAS 2022), 2022.

https://doi.org/10.1021/acssensors.3c00256
ACS Sens. 2023, 8, 2572−2582